IEEE Open Journal of
Industry Applications

Received 14 March 2024; revised 24 June 2024; accepted 5 September 2024. Date of publication 13 September 2024;
date of current version 30 September 2024. The review of this article was arranged by Associate Editor Marco Di Benedetto.

Digital Object Identifier 10.1109/OJIA.2024.3460669

Model Predictive Control in Multilevel Inverters Part I: Basic Strategy and Performance Improvement

CRISTIAN GARCIA [1] (Senior Member, IEEE), ANDRES MORA [2] (Member, IEEE), MARGARITA NORAMBUENA [2] (Senior Member, IEEE), JOSE RODRIGUEZ [3] (Life Fellow, IEEE), MOKHTAR ALY [3] (Senior Member, IEEE), FERNANDA CARNIELUTTI [4] (Member, IEEE), JAVIER PEREDA [5] (Senior Member, IEEE), PABLO ACUNA [1] (Member, IEEE), RICARDO AGUILERA [6] (Member, IEEE), AND LUCA TARISCIOTTI [7] (Senior Member, IEEE)

(Invited Paper)

[1]Department of Electrical Engineering, Universidad de Talca, Curico 3340000, Chile
[2]Department of Electrical Engineering, Universidad Tecnica Federico Santa Maria, Valparaiso 30332, Chile
[3]Department of Engineering Sciences, Universidad San Sebastian, Santiago 30332, Chile
[4]Campus Santa Maria and Power Electronics and Control Research Group (GEPOC), UFSM, Federal University of Santa Maria, Santa Maria 97105-900, Brazil
[5]Department of Electrical Engineering, Pontificia Universidad Católica de Chile, Santiago 8331150, Chile
[6]School of Electrical and Data Engineering, at the University of Technology Sydney, Broadway, NSW 2007, Australia
[7]Department of Engineering Sciences, University Andres Bello, Santiago 7550196, Chile

CORRESPONDING AUTHOR: ANDRES MORA (e-mail: andres.mora@ usm.cl).

This work was supported in part by ANID through projects Fondecyt under Grant 1241099, Grant 1210208, Grant 1221239, Grant 1231030, Grant 1240046, Grant 1231265, and Grant 1230250, in part by ANID/ANILLO/ATE230035, and in part by the ANID Basal Project FB0008 Advanced Center for Electrical and Electronic Engineering.

ABSTRACT Multilevel inverters (MLIs) have lately become important due to their extended application to electrical transmission and distribution systems. At the same time, the control and modulation of MLIs are especially challenging due to the high number of switching states, many of them redundant in terms of output voltage generation, and their nonlinear characteristics. In order to ease their implementation in real environment, model predictive control (MPC) is often considered, where the main control targets are: 1) to generate a the desired output current and 2) to keep the internal converter capacitor voltages at their reference value. However, a major issue with the implementation of MPC in MLIs is that the number of calculations to be done online increases dramatically with the number of levels, making it almost impossible to apply MPC in some practical cases. For these reasons, one of the main research trend in MPC for MLIs is to provide an algorithm which can reduce the computational burden necessary to operate the control. The article proposes a review of such control techniques. Starting from the basic MPC implementation and using a flying capacitor converter as an example the article review the basic strategies to avoid calculating the weighting factor in the cost function, simplifying the implementation. Also, methods to reduce the number of calculations necessary to implement MPC are shown and applied to cascaded H-bridge converters. These techniques allow to keep an high load current quality while reducing more than 95% in the number of calculations necessary to implement the control. Finally, other operation improvements of MPC are also included, such as fixed switching frequency operation and multistep MPC, reaching an important performance improvement compared to the basic MPC strategy.

INDEX TERMS Model predictive control (MPC), multilevel inverters (MLIs).

I. INTRODUCTION

Multilevel inverters (MLIs) are structures of power electronic devices and passive components that allow the generation of several voltage level at their output. Lately industry have shown interest in these structures, especially when applied to electrical transmission lines, sustaining their development in the last two decades [1], [2], [3], [4], and allowing to reach the medium voltage level at power in the range of Megawatts [3], [4]. At the same time, another important attribute of MLIs is that they can generate high quality waveform also at the low voltage levels, thus reducing the need of passive filters and the overall converter size. For such reason lately MLIs have been applied to a wide variety of low voltage applications, such as photovoltaic (PV) [5], [6], [7], [8], [9] and wind generation [10], [11]. Finally, the potential application of MLI in the car industry have also been explored [12], [13], [14] as well as development of new typologies that have been published recently [15], [16], [17], [18], [19]. In terms of control for MLIs, linear controllers with carrier-based pulsewidth modulation (PWM) [20], [21], [22], space vector modulation [23], direct torque control [24], [25], and optimized pulse patterns [26] are the preferred techniques in industry. In the last years, with the availability of fast and powerful microprocessors, new and more modern techniques are showing increasing application in MLI. Some of these techniques are: 1) passivity based [27], 2) sliding mode [28], [29], [30], and 3) artificial neural networks [31], [32], [33]. In addition, model predictive control (MPC) has been recently proposed, finding increasing attention in power electronics. The most attractive features of MPC are: 1) it is simple to understand and to implement, 2) it can consider very easily model nonlinearities and control constraints, and 3) it can control simultaneously a wide variety of variables [34], [35], [36], [37], [38], [39], [40]. Lately, the application of MPC in MLIs is being studied intensively [41], [42], [43], [44], [45], [46], [47] in order to address the higher complexity of the power circuit, especially in hybrid MLIs, which makes it more difficult to develop any control strategy. However, the application of MPC in MLIs demands a very high number of calculations that increase dramatically with a higher number of levels, making this alternative almost unrealistic in many applications [48], [49]. A first attempt to recollect possible solution for the implementation of MPC in MLIs has been carried out in [50], where MPC strategies are categorized in two groups, direct MPC (without modulator) and indirect MPC (with modulator), presenting in a very clear and systematic way the recent advances of each of them. Another important contribution is a complete classification of methods to design the weighting factors in the cost function.

This work extends the one in [50], and it is divided into two review papers (Part I and Part II), which are complementary to the approach presented in [50]. The work is divided into two main sections in this first part of the review. In Section II, the basic strategy of MPC applied to MLIs is reviewed and applied to a flying capacitor (FC) converter, using the basic instantaneous equations of the converter and establishing a very systematic and clear relation between the gate drive signals of the power switches and the variables to be controlled, such as the load current and the capacitor voltages. Several implementations of finite control-set (FCS) MPC are proposed for the FC converter, and modifications to the FCS-MPC algorithm to reduce the required computational effort are analyzed. In Section III, special attention is given in this article to the presentation of strategies that significantly reduce the number of commutations when using MPC in MLIs with a high number of levels, considering the case of cascaded H-bridge (CHBs) converters, which present a high level of states redundancy. To achieve this target, this article presents a technique that generates an important reduction in the number of commutations by introducing an additional term in the cost function. This modification reduces the switching losses compared to basic MPC. Finally, multistep MPC (MS-MPC) is introduced as a promising novel predictive control technique.

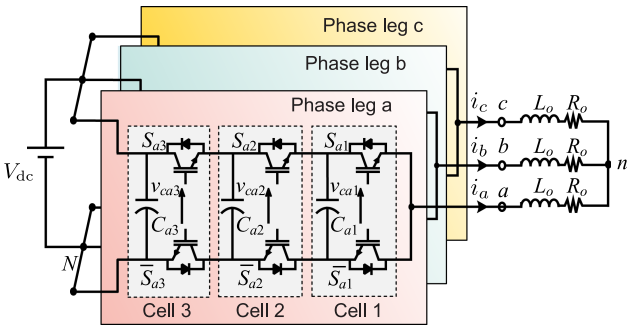

FIGURE 1. Power circuit of four-level FC-MLI topology.

II. FCS-MPC STRATEGIES FOR COMPUTATIONAL BURDEN REDUCTION

In this section, the basic operating principle of the FCS-MPC strategy is introduced and then advanced techniques to reduce the control computational burden are reviewed. A four-level FC MLI topology is selected as a case study for introducing the basic MPC method, since it includes all the complexities of an MLI control, such as multiple control targets, redundancy of states, and necessity of constraints. Starting from the FC and load model, the states prediction are depicted and several FCS-MPC implementations are analyzed, in order to assess the multiobjective control capability and assess the computational burden required by the control algorithm in various implementations.

The power circuit of the three-phase four-level FC-MLI topology with R–L load is shown in Fig. 1. Each FC cell is composed of one capacitor and two complementary switches. The capacitor voltages ratio is preserved at $v_{cx1} : v_{cx2} : v_{cx3} = 1 : 2 : 3$, where $x \in \{a, b, c\}$. Based on this ratio, each phase leg can output four different voltage levels among the output terminal of phase x and the neutral point N of the inverter. Table 1 shows the various switches combination and the corresponding output voltage levels in each phase. Each phase leg can generate eight switching states, and each of the

TABLE 1. Switching States of the FC Converter

State	Output		Switch Pulses		
	Level	v_{xN}	S_{x1}	S_{x2}	S_{x3}
1	0	0	0	0	0
2	$\frac{V_{dc}}{3}$	$V_{dc} - v_{cx2}$	0	0	1
3		$v_{cx2} - v_{cx1}$	0	1	0
4		v_{cx1}	1	0	0
5	$\frac{2V_{dc}}{3}$	v_{cx2}	0	1	1
6		$V_{dc} - v_{cx2} + v_{cx1}$	1	0	1
7		$V_{dc} - v_{cx1}$	1	1	0
8	V_{dc}	V_{dc}	1	1	1

voltage levels $2V_{\rm dc}/3$ and $V_{\rm dc}/3$ has three redundant switching states.

A. MODELING OF THE TOPOLOGY

Based on the switching states in Table 1, the mathematical model of the instantaneous output voltage of each inverter leg can be represented as follows:

$$v_{xN} = S_{x3}V_{\rm dc} - (S_{x3} - S_{x2})v_{cx2} - (S_{x2} - S_{x1})v_{cx1} \tag{1}$$

where the switch signals S_{x1}, S_{x2}, and S_{x3} equal to 1 mean ON state and 0 mean OFF state.

In addition, the instantaneous capacitor voltages can be represented as follows:

$$v_{cx1} = v_{cx1}(0) + \frac{1}{C_{x1}}\int_0^t i_x(S_{x2} - S_{x1})(\tau)\mathrm{d}\tau \tag{2}$$

$$v_{cx2} = v_{cx2}(0) + \frac{1}{C_{x2}}\int_0^t i_x(S_{x3} - S_{x2})(\tau)\mathrm{d}\tau \tag{3}$$

where i_x represents the instantaneous output current of phase x. At the same time, the dynamical modeling of the four level FC-MLI topology with R–L load can be obtained using the Kirchhoff voltage law. The continuous time modeling of the inverter output can be represented for each phase leg as follows:

$$v_{xN} = R_o i_x + L_o\frac{\mathrm{d}i_x}{\mathrm{d}t} + v_{nN} \tag{4}$$

where R_o represents the load resistance and L_o represent the load inductance for the star-connected three-phase load. v_{nN} denotes to the estimated common-mode voltage (CMV) for the inverter output between the neutral point of the load n and the negative terminal of the dc input side N. Therefore, the continuous time dynamical modeling of the three phases can be represented using (4) as follows:

$$\frac{\mathrm{d}}{\mathrm{d}t}\begin{bmatrix} i_a \\ i_b \\ i_c \end{bmatrix} = -\frac{R_o}{L_o}\begin{bmatrix} i_a \\ i_b \\ i_c \end{bmatrix} + \frac{1}{L_o}\begin{bmatrix} V_{aN} \\ V_{bN} \\ V_{cN} \end{bmatrix} - \frac{1}{L_o}\begin{bmatrix} V_{nN} \\ V_{nN} \\ V_{nN} \end{bmatrix} \tag{5}$$

where the CMV v_{nN} is given as follows:

$$v_{nN} = \frac{1}{3}(v_{aN} + v_{bN} + v_{cN}). \tag{6}$$

By substituting from (6) into (5), state-space modeling for the four-level FC-MLI topology is expressed as follows:

$$\frac{\mathrm{d}}{\mathrm{d}t}\begin{bmatrix} i_a \\ i_b \\ i_c \end{bmatrix} = -\frac{R_o}{L_o}\begin{bmatrix} i_a \\ i_b \\ i_c \end{bmatrix} + \frac{1}{3L_o}\begin{bmatrix} 2 & -1 & -1 \\ -1 & 2 & -1 \\ -1 & -1 & 2 \end{bmatrix}\begin{bmatrix} V_{aN} \\ V_{bN} \\ V_{cN} \end{bmatrix}. \tag{7}$$

B. PREDICTION STAGE

The prediction of the output current and capacitor voltages represents the first stage in FCS-MPC methods. In which, the future states for the topology are predicted for all of the possible inverter switching states. Due to the sampling property of FCS-MPC methods, the discrete time modeling is utilized in this stage. The Euler approximation approach is employed to represent the predicted future states. The predicted output currents of the inverter can be modeled using (7) as follows:

$$\boldsymbol{i}^{k+1}_{\rm abc} = \mathbf{A}\boldsymbol{i}^{k}_{\rm abc} + \mathbf{B}\boldsymbol{v}^{k}_{\rm abc} \tag{8}$$

where $\mathbf{A}$ and $\mathbf{B}$ are the state-space matrices, given by

$$\mathbf{A} = \mathrm{diag}\left[1 - \tfrac{T_s R_o}{L_o} \quad 1 - \tfrac{T_s R_o}{L_o} \quad 1 - \tfrac{T_s R_o}{L_o}\right] \tag{9}$$

$$\mathbf{B} = \frac{T_s}{3L_o}\begin{bmatrix} 2 & -1 & -1 \\ -1 & 2 & -1 \\ -1 & -1 & 2 \end{bmatrix} \tag{10}$$

where T_s denotes the sampling time period of the FCS-MPC algorithm. The capacitor voltages can be predicted as follows:

$$v^{k+1}_{cx1} = v^{k}_{cx1} + \frac{T_s}{C_{x1}}i^{k}_{x}\left(S^{k+1}_{x2} - S^{k+1}_{x1}\right) \tag{11}$$

$$v^{k+1}_{cx2} = v^{k}_{cx2} + \frac{T_s}{C_{x2}}i^{k}_{x}\left(S^{k+1}_{x3} - S^{k+1}_{x2}\right). \tag{12}$$

C. BASIC FCS-MPC STRATEGY

One main advantage of the FCS-MPC method is the incorporation of multiple objectives in a single cost function. For the four-level FC-MLI topology, the output currents of the three phases and the capacitor voltages in each phase leg are included in the cost function. The cost function g^k_{iv} of the basic FCS-MPC method can be represented as follows:

$$g^k_{iv} = \lambda_i \sum_{x\in\mathcal{P}}\left(i^*_x - i^{k+1}_x\right)^2 + \lambda_{c1}\sum_{x\in\mathcal{P}}\left(v^*_{c1} - v^{k+1}_{cx1}\right)^2 + \lambda_{c2}\sum_{x\in\mathcal{P}}\left(v^*_{c2} - v^{k+1}_{cx2}\right)^2 \tag{13}$$

where $\mathcal{P} = \{a, b, c\}$; and λ_i, λ_{c1}, and λ_{c2} denote to the weighting factors of FCS-MPC for the inverter output currents, the capacitor C_{x1} voltages, and the capacitor C_{x2} voltages, respectively. The weighting factors λ_i, λ_{c1}, and λ_{c2} are responsible for distributing the effort of the control algorithm among the output current and capacitor voltages. Whereas, i^{k+1}_x, v^{k+1}_{cx1}, and v^{k+1}_{cx2} represent the predicted states for the various switching states of the inverter. The term i^*_x represents the reference

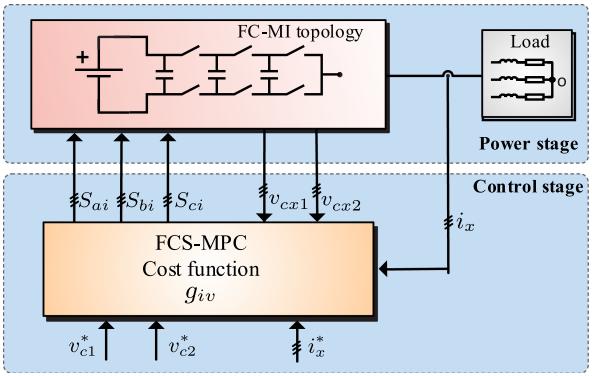

FIGURE 2. Block diagram of basic FCS-MPC method.

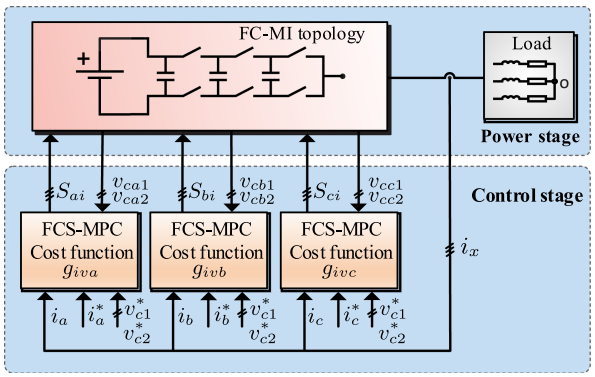

FIGURE 3. Block diagram of single-phase FCS-MPC method.

output currents for the inverter. The reference voltages for capacitors v_{c1}^* and v_{c2}^* are set based on the operation of the topology as follows:

$$v_{c1}^* = \frac{V_{\rm dc}}{3} \quad \text{and} \quad v_{c2}^* = \frac{2V_{\rm dc}}{3}. \tag{14}$$

Afterward, the calculation of objective function g_{iv}^k is made for the available switching states (with eight switching states in each phase that result in having $8^3 = 512$ total states) in each sampling instant. Then, the FCS-MPC algorithm selects the optimum switching state that achieves minimized objective function of all the controlled variables. Finally, the gating pulses that correspond to the optimum objective function are applied to the inverter based on Table 1. Fig. 2 shows the block diagram of the basic FCS-MPC strategy applied to the four-level FC-MLI.

D. SINGLE-PHASE CONTROL STRATEGY

The idea behind this strategy is to consider the CMV as a constant and consequently implementing the FCS-MPC in each phase of the converter independently. Thus, the total possible switching states for a four-level FC-MLI will be $8 \times 3 = 24$ instead of $8^3 = 512$ in the basic FCS-MPC. To do this approximation, it is necessary that the system has some specific characteristics.

Assuming symmetrical sinusoidal output currents, the converter output voltages can be rewritten in terms of their spectral components as follows:

$$v_{aN} = \frac{V_{\rm dc}}{2} + A_1 \sin(\omega_o t + \phi) + {\rm HF}_a \tag{15}$$

$$v_{bN} = \frac{V_{\rm dc}}{2} + A_1 \sin\left(\omega_o t - \frac{2\pi}{3} + \phi\right) + {\rm HF}_b \tag{16}$$

$$v_{cN} = \frac{V_{\rm dc}}{2} + A_1 \sin\left(\omega_o t + \frac{2\pi}{3} + \phi\right) + {\rm HF}_c \tag{17}$$

where A_1 is the fundamental component of v_{xN}, ${\rm HF}_x$ are the high-frequency components, which depend on the selected switching pattern, and ϕ depends on the fundamental phase shift. Therefore, considering (15)–(17) and the definition of v_{oN}, the CMV can be rewritten as

$$v_{oN} = \frac{V_{\rm dc}}{2} + \widetilde{\rm HF}_x \tag{18}$$

where $\widetilde{\rm HF}_x$ is a combination of the high-frequency components of the output phases. It is important to remark that, due to the low-pass filtering effect of most loads, these high-frequency components have a reduced effect in the output currents. Therefore, (4) can be approximated by

$$v_{xN} \approx R_o i_x + L_o \frac{{\rm d}i_x}{{\rm d}t} + \frac{V_{\rm dc}}{2}. \tag{19}$$

By using this approach, the system can be approximated as three independent single-phase systems and the cost function for each phase $x \in \{a, b, c\}$ will be

$$g_{ivx} = \left(i_x^* - i_x^{k+1}\right)^2 + \lambda \left[\left(v_{c1}^* - v_{cx1}^{k+1}\right)^2 + \left(v_{c2}^* - v_{cx2}^{k+1}\right)^2\right] \tag{20}$$

where λ is a weighting factor used to emphasize either the current or the voltage tracking.

Finally, the voltage vector that minimizes (20) for each phase is applied at the beginning of the next sample time, $k+1$. Fig. 3 shows the block diagram of the single-phase FCS-MPC strategy.

The single-phase control strategy sacrifices common mode variable observation in front of computational cost. This means that independent phase control could have a high variation in the CMV without possible action to correct it and, consequently, more harmonics in the output spectrum.

E. SPLIT CONTROL IN CONVERTER AND LOAD INDEPENDENTLY

One of the characteristics of multilevel converters is their redundant states. These are valid when the inner voltages of the converters are kept in the neighborhood of their desired values. In the case of the four-level FC-MLI, there are three redundant states for each medium range output voltage, and only in these states the inner capacitors voltages are affected. The voltage dynamics in the inner capacitors are considerably slower than the output current dynamics, and if the sampling time is fast enough, it is possible to assume that the inner

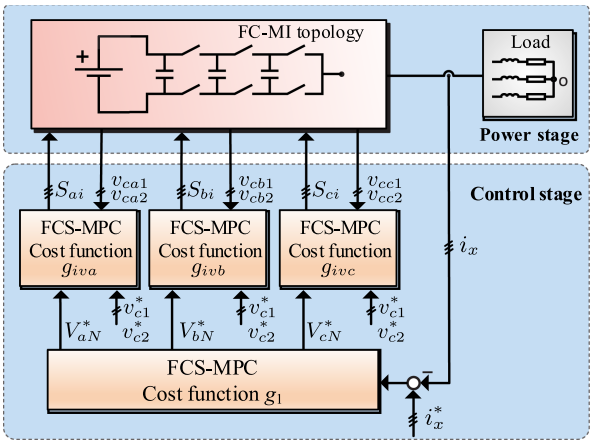

FIGURE 4. Block diagram of split FCS-MPC method.

voltages are kept almost constant in every sampling time, and the variation and influence in the current control loop is small enough to be neglected.

Thus, to reduce the computational cost, this strategy separates the whole problem into two different control problems: one for the load and its constraints (current tracking error) and another for the converter and its constraints (inner voltages tracking error). As a result, this FCS-MPC strategy has two separate problems with two different cost functions. Further details can be found in [51].

The FCS-MPC associated to the load uses the output voltage levels, that in the case of FC-MI are four, to predict the possible state in the FCS-MPC algorithm through (8)–(10). This is possible considering that the capacitors are close to the balanced point. Thus, the cost function is

$$g_1^k = \left(i_a^* - i_a^{k+1}\right)^2 + \left(i_b^* - i_b^{k+1}\right)^2 + \left(i_c^* - i_c^{k+1}\right)^2 \quad (21)$$

where i_x^{k+1} is the predicted current for the phase $x \in \mathcal{P}$.

The output of this stage is the output voltage level required for each phase. If the output voltage level is one of the middle level with redundant switching states, the control of the converter to balance the inner capacitor is used considering (11) and (12). In this stage, the control is split for each phase, as different phases could have different output voltage level references. Using (1), the switching state for each possible output voltage is selected. In this case, the cost function for each phase x is given by

$$g_{2x}^k = \left(v_{c2}^* - v_{2x}^{k+1}\right)^2 + \left(v_{c1}^* - v_{1x}^{k+1}\right)^2. \quad (22)$$

Fig. 4 shows the block diagram for the split FCS-MPC strategy. The output of this stage is the switching state that generates the balanced output voltage.

F. GLOBAL ASSESSMENT OF CONTROL STRATEGIES

To compare the strategies for reducing the computational cost in the basic FCS-MPC, the single-phase FCS-MPC and split FCS-MPC control with four-level FC-MLI are considered. The total *dc-link* is set to 300 V, and the load is $L_o = 10$ mH and $R_o = 15\,\Omega$. The sampling period is $T_s = 100\,\mu$s. Fig. 5 shows the simulation results for a current step from $i_{\text{ref}} = 3\sin(\omega t)$ to $i_{\text{ref}} = -7\sin(\omega t)$, this is a step in a reference magnitude and a 180° change in the phase. It is possible to see from Fig. 5 that all MPC strategies achieve a fast and good performance during this dynamic step. In the steady-state performance, the basic FCS-MPC has a 2.86% total harmonic distortion (THD) in the output current, the single-phase FCS-MPC has a 3.66% output current THD and the split FCS-MPC has a 2.92% output current THD. Table 2 shows the THD of the output current for the different control strategies and the necessary number of iterations to obtain the switching state that minimizes the cost function. Fig. 6 shows a comparison of the execution times of the three methods. All control methods were executed on a standard commercial control platform Launchpadxl-F28379D (200 MHz). From this analysis, it can be seen that the basic FCS-MPC requires an execution time of 2996 μs, the Split method 220 μs and the single-phase FCS-MPC 66 μs. From this result, it is possible to conclude that the basic FCS-MPC method is not directly implementable for high-level count converters and that the use of computational cost reduction strategies is crucial.

TABLE 2. THD and Number of Calculations With Different MPC Strategies

Control Scheme	THD for Output Current	Number of Iterations
Basic FCS-MPC	2.86%	512
Split FCS-MPC	2.92%	64
Single-phase FCS-MPC	3.66%	24

G. OTHER ADVANCED STRATEGIES

In order to reduce the computational burden of FCS-MPC strategies applied to MLIs some methods have been presented in literature, such as sphere decoding [53], branch and bound [54], [55], FCS-MPC without weighting factors [56], [57], [58] and multiple-voltage-vector MPC [52], [59].

Table 3 shows a resume of different strategies that can reduce the number of calculations using a reduced selection of the total switching states of the inverter. As an example, let us consider the multiple-voltage-vector MPC shown in Fig. 7 and presented in [52] and [59] for a three-level T-type converter. First, the voltage reference is calculated and then transformed to the first sector of the space-vector diagram, and only the vectors that are closer to the reference are considered for the optimization problem. A switching sequence is implemented during each sampling period, and the dwell times of the voltage vectors are calculated according to a cost function. As the neutral point voltage can be balanced by using redundant voltage vectors in the same switching sequence, the strategy is further simplified by excluding from the cost function the parcel relative to the balance of the neutral point voltage, considering only the current tracking error. This eliminates the need for more calculations and the use of weighting factors.

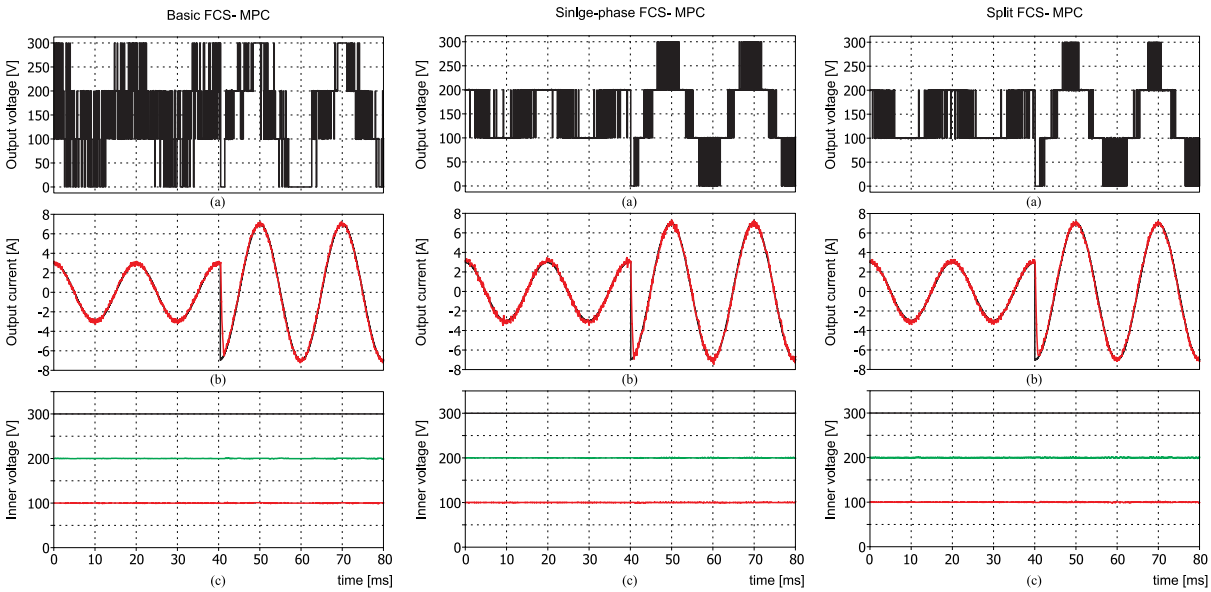

FIGURE 5. Comparison results for a step current reference from $3A_{peak}$ to $7A_{peak}$, four-level FC-MLI. (a) Output voltage V_{aN}. (b) Output current i_a. (c) Inner voltage in capacitors phase a, v_{ca1}, and v_{ca2}.

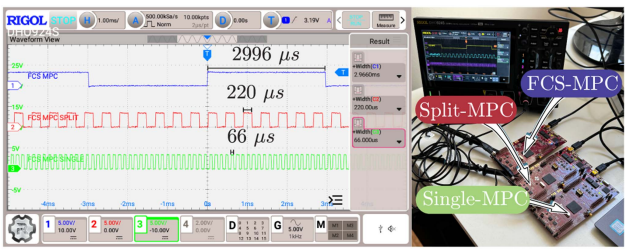

FIGURE 6. Comparison of execution times of the control methods basic FCS-MPC, single-phase FCS-MPC, and split FCS-MPC. (a) Measurement of execution times. (b) Evaluation test.

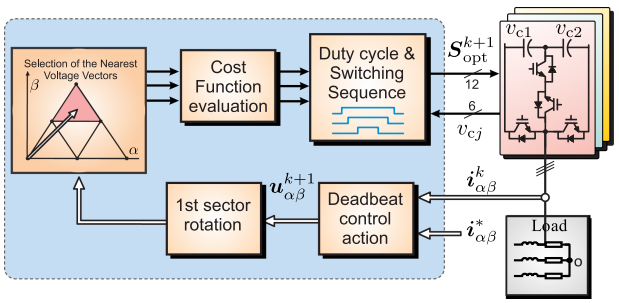

FIGURE 7. Multiple-voltage-vector MPC [52].

Other FCS-MPC algorithms with an implicit modulator for neutral point clamped (NPC) converters have been proposed in [60], [61], [62], and [63].

III. FCS-MPC STRATEGIES FOR LOW-SWITCHING FREQUENCY

In this section, an FCS-MPC with reduction of the number of commutations will be discussed, considering as an example a three-phase 11-level CHB inverter. This topology is modular

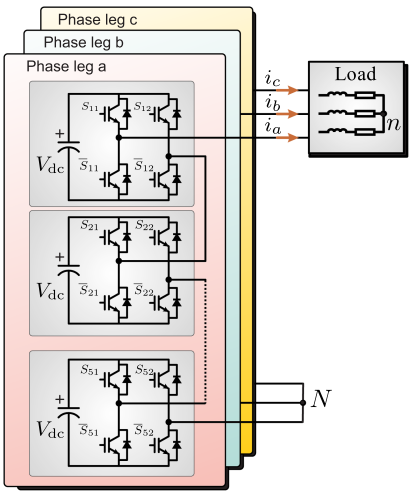

FIGURE 8. Power circuit of an 11-level three-phase CHB topology.

and a different number of series-connected cells can be used to reach various medium voltage levels. The schematic diagram of the inverter is shown in Fig. 8. Each cell has four switches and an isolated dc source, usually generated by phase-shifting power transformers followed by diode rectifiers. The switching state of each cell is represented by $S_{xi} \in \{1, 0, -1\}$, where $x \in \{a, b, c\}$ denotes the three-phase system, and $i \in \{1, ..5\}$ is the cell's index.

Assuming that the isolated dc sources are identical and hold equal dc voltages V_{dc}, the output voltage of each cell is $S_{xi}V_{dc}$. The total output voltage of each phase V_{xN} equals the summation of the outputs of the individual cells as

$$V_{xN} = \sum_{i=1}^{5} S_{xi} V_{dc}. \tag{23}$$

TABLE 3. Resume of Strategies to Reduce the Number of Calculations

Strategy	Main characteristic
Sphere Decoding Algorithm (SDA) [53]	• Considers a long prediction horizon. • The optimal sequence is selected using a branch and bound algorithm. • To avoid variable computational time, partial graph processing is used.
Hierarchical Model Predictive Control [54]	• The strategy is divided into three steps. • First step is the optimization problem, divided into two sub-optimal MPC problems, one for the load and one for the inverter. • Second step is the global optimal vector selection. • Last step selects the global optimal redundant vector using the converter-specific characteristics, like capacitor voltage balance.
Branch and Bound MPC [55]	• Also a three steps strategy. • First step is the linear coordinate transformation. • Second step is vector entries selected as a branch. • Last step is the selection of the global optimal integer result.
Multi-step FCS-MPC [56]–[58]	• The optimization problem is reformulated as a $l2$ norm optimization problem without cost functions and weighting factors. • Directly calculates the optimal converter voltage vector in order to minimize both the current tracking error and the converter common-mode voltage
Multiple-Voltage-Vector MPC [52], [59]	• Results in fixed switching frequency. • A switching sequence is implemented during each sampling period. • The redundant voltage vectors are used to balance inner variables of the inverter.
Fast MPC [64]	• The system model is written in the line-to-line voltages coordinates, where the inverter voltage vectors have only integer entries. • The voltage reference vector is truncated into the nearest inverter voltage vector, such as to minimize the current tracking error. • A second cascaded optimization problem is solved to chose which redundant state of the inverter voltage vector will be implemented to balance the voltages of the inner capacitors.
Space Vector Modulated MPC [65]	• Results in fixed switching frequency. • Combines control and modulation in a convex optimization problem with affine inequality constraints to minimize the tracking errors of the output variables. • Using the Karush–Kuhn–Tucker conditions, feasible duty cycles are computed for both linear and overmodulation regions.
Fast Optimal MPC [66]	• The dynamic equations are used to predict the future values of the control variables in order to keep the voltages of the capacitors balanced. • Once the reference voltage vector is calculated, the distance between it and the 27 NPC voltage vectors is calculated, and the one closer to the reference is chosen to be implemented.
"S" Factor Scheme [67]	• First, a reduced number of possible vectors is selected considering the inverter variables (balance of the inner capacitors voltages). • The reference voltage vector is predicted using the model. • The nearest vector to the reference (considering the first step) is selected

A. FCS-MPC WITH FEW COMMUTATIONS

Considering a three-phase $R-L$ load, the load model derived in (4)–(10) for the FC converter is also valid in this case study. However, CHB differs from FC in commutation patter and redundancy, which is in the scope of this section. In particular, it is well known that the number of commutations in the power switches impacts the switching frequency and the power losses and an higher number of commutations results in higher switching frequency and power losses. For this reason, it is very important to reduce the number of commutations. In a multilevel converter, such as the 11-level CHB, it is possible to reduce the switching commutations due to the high number of available output voltage levels to generate the desired output voltage, i.e., the voltage vector redundancies.

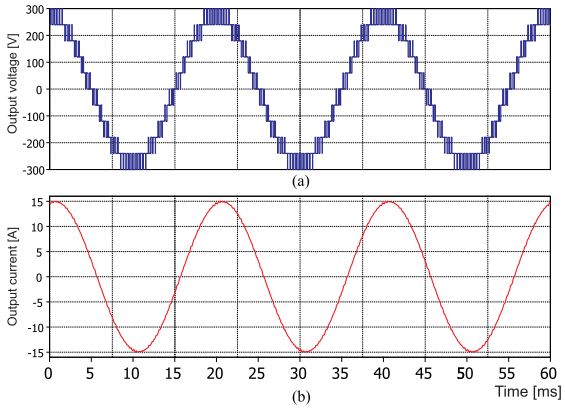

FIGURE 9. Classical PS-PWM, current reference 15A, 11-levels CHB. (a) Output voltage V_{aN}. (b) Output current i_a.

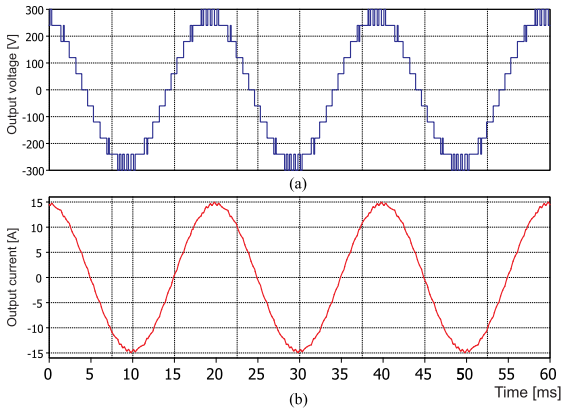

FIGURE 10. FCS-MPC with few commutations, current reference 15A, 11L-CHB. (a) Output voltage V_{aN}. (b) Output current i_a.

A simple cost function can be designed to control the number of switching commutations, such as

$$g = \sum_{x \in \mathcal{P}} \left(i_x^* - i_x^{k+1} \right)^2 + \lambda \left(V_{xN}^k - V_{xN}^{k+1} \right)^2 \tag{24}$$

where λ is the weighting factor, V_{xN}^k is the output voltage at sampling time k and V_{xN}^{k+1} is the predicted output voltage for the next sampling time for all $x \in \{a, b, c\}$, written as

$$V_{xN} = V_{\text{dc}} \big(S_{x11} + S_{x21} + S_{x31} + S_{x41} + S_{x51} - S_{x12} - S_{x22} - S_{x32} - S_{x42} - S_{x52} \big). \tag{25}$$

As the equation that describes the output voltage depends on the switching states, it is possible to reduce the switch commutation by reducing the changes on the output voltage levels. It is possible to see from (25) that a step of one level in the output voltage means that one power switch changes its state and a step of two levels in the output voltage means that two power switches change.

In order to verify the theoretical analysis, the three-phase 11-level CHB inverter was simulated using the classical phase-shifted PWM (PS-PWM) modulation and the FCS-MPC with reduced number of commutations. The total dc-link voltage is set to 300 V, and the load is $L_o = 10$ mH and $R_o = 15\,\Omega$. The sampling period is $T_s = 100\,\mu$s. Figs. 9 and 10 show, respectively, the simulation results for the PS-PWM and the FCS-MPC with reduced number of commutations. It is possible to see from these results that the FCS-MPC works properly, even with less number of commutations.

Fig. 11 shows the effect of the weighting factor on the number of commutations and the THD of the output current. It is clear that a low value of the weighting factor produces a low THD but also results in a high number of total commutations. However, a high value of the weighting factor produces a high distortion in the output currents and a low number of commutations. Considering this graphic, the selected weighting factor is $\lambda = 0.000048$. Finally, Table 4 shows the average number of commutations in one period of the fundamental voltage for each strategy. It can be seen that the classical PS-PWM has

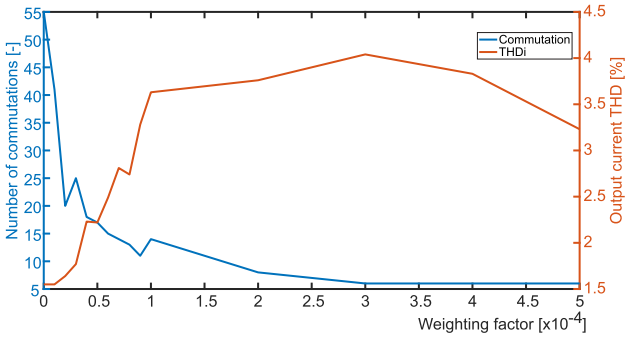

FIGURE 11. Commutation number and THD in the output current in the function of the weighting factor.

TABLE 4. THD and Number of Commutations With Different MPC Strategies

Control Scheme	THD for Output Current	Number of Commutations
Classical PS-PWM	2.01%	69
Reduced FCS-MPC	2.62%	23

triple the commutations for a very similar performance than the FCS-MPC with reduced number of commutations.

B. MULTISTEP MPC

In recent years, MS-MPC has taken notable steps toward improving steady-state performance of MLIs while retaining the fast dynamic performance provided by its single-step counterpart. The benefits of MS-MPC can be mainly appreciated in high power MLIs that normally operate at low switching frequency [41], [68], [69], [70], [71]. For instance, Table 5 shows experimental results for an MLI, demonstrating a reduction in the THD of the load current while achieving a similar average device switching frequency [72]. Advantages can be also observed in high-order systems, e.g., inverters with *LC* filters, where MS-MPC has been shown to reduce oscillations due to filter resonance [73]. Generally in MS-MPC, a single-step cost function is expanded to add N system state predictions;

TABLE 5. Example of Experimental Steady-State Performances in MLIs

Horizon length	$N=1$	$N=1$	$N=3$
Weighting factor	$\sigma=0$	$\sigma=10^{-6}$	$\sigma=10^{-6}$
Optimizer	ESA	SDA	SDA
Execution Time, T_e (% of T_s)	39.8%	11.1%	92.2%
THD of the load currents, THD_i	4.01%	4.03%	3.36%
Standard deviation of CMV, v_{0n}^{δ}	64.5 V	48.51 V	47.7 V
Inverter voltage symmetry, $\mathcal{S}_m$	0.57	0.88	0.92
Avg. device switching freq., f_{sw}	387.5 Hz	331.25 Hz	334.12 Hz

e.g.,

$$J_N=\sum_{k=0}^{N-1}\|\boldsymbol{x}(k+1)-\boldsymbol{x}^{\star}(k+1)\|_2^2+\lambda\|\boldsymbol{u}(k)-\boldsymbol{u}(k-1)\|_2^2 \tag{26}$$

where $\lambda>0$ is a weighting factor used to limit the converter voltage level transitions thus reducing the switching frequency. Then, the following multistep optimal control problem is solved

$$\begin{aligned}&\boldsymbol{U}_{\text{opt}}(k)=\arg\{\min J_N(k)\}\\&\text{subject to: }\boldsymbol{u}(k)\in\mathbb{U}\end{aligned} \tag{27}$$

where $\mathbb{U}$ represents the FCS. This minimization leads to the following multistep optimal control input vector:

$$\boldsymbol{U}_{\text{opt}}(k)=\begin{bmatrix}\boldsymbol{u}_{\text{opt}}^{\text{T}}(k) & \cdots & \boldsymbol{u}_{\text{opt}}^{\text{T}}(k+N-1)\end{bmatrix}^{\text{T}}. \tag{28}$$

Finally, only the first control action in (28), i.e., $\boldsymbol{u}_{\text{opt}}(k)$, is applied to the system.

Despite the aforementioned benefits that MS-MPC offers to control MLIs, there are still open challenges, such as computation burden reduction. This is particularly important in MLIs since the number of computations exponentially increases with the number of switch combinations, voltage output levels, and the prediction horizon N. To tackle this issue, literature shows a clear tendency to reformulate the MS-MPC problem into an integer least squares optimization problem, given by

$$\boldsymbol{U}_{\text{opt}}(k)=\arg\left\{\min_{\boldsymbol{U}(k)\in\mathbb{U}^N}\|\boldsymbol{H}\boldsymbol{U}(k)-\bar{\boldsymbol{U}}_{\text{unc}}(k)\|_2^2\right\} \tag{29}$$

where $\boldsymbol{H}$ is a triangular matrix formed by using the system model and weighting factors; see [68] and [72]. It is important to highlight that solving (29) leads to the same optimal solution, $\boldsymbol{U}_{\text{opt}}(k)$, as per (28). Favorably, with this reformulation, it is possible to use a computationally efficient sphere decoding algorithm (SDA) to find $\boldsymbol{U}_{\text{opt}}(k)$ in the transformed space generated by matrix $\boldsymbol{H}$. The SDA working principle is based on initially forming a sphere centred in the unconstrained optimal solution $\bar{\boldsymbol{U}}_{\text{unc}}$, and an initial candidate vector $\boldsymbol{U}_{\text{ini}}$.

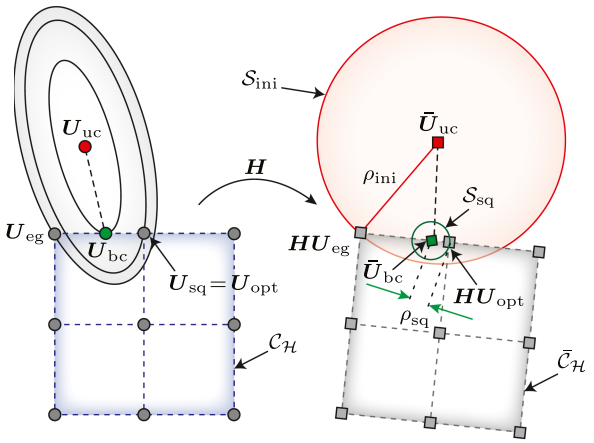

FIGURE 12. Graphical representation of the MS-MPC problem (an FCS $\mathbb{U}$ of nine control input vectors) during transient in the original space, and transformed space generated by $\boldsymbol{H}$ [74].

This results in a sphere with radius $\rho_{\text{ini}}^2=\|\boldsymbol{H}\boldsymbol{U}_{\text{ini}}-\bar{\boldsymbol{U}}_{\text{unc}}\|_2^2$. Then, all vectors that lie outside this initial sphere can be quickly discarded by the SDA. If a new vector is found to be inside the sphere, it is then chosen to form a new smaller sphere. This process is thus repeated until the sphere cannot be further shrunk, which implies the optimal solution $\boldsymbol{U}_{\text{opt}}$ has been found. MS-MPC using SDA has been proposed in literature to control MLI for electrical drives [75], inverters with *LC(L)* filters [74], [76], [77], and other applications [78].

Recently, it has been shown that even though this SDA implementation can efficiently solve MS-MPC for MLI working close to a steady-state operation, there is a crucial computational burden issue that arises when finding the optimal solution during transient operations [79]. This situation is graphically illustrated in Fig. 12. During transients, a large actuation is normally required to drive the currents close to their references. This result in a large value of $\bar{\boldsymbol{U}}_{\text{unc}}$, which in this case lies far away from the FCS border $\bar{\mathcal{C}}_{\mathcal{H}}$. To address this issue, in [80] the SDA was preconditioned by projecting $\bar{\boldsymbol{U}}_{\text{unc}}$ onto $\bar{\mathcal{C}}_{\mathcal{H}}$. This is achieved by obtaining a box-constrained optimal solution of (29), i.e., $\bar{\boldsymbol{U}}_{\text{bc}}\in\bar{\mathcal{C}}_{\mathcal{H}}$. Then, an initial candidate is obtained by sequentially quantizing $\bar{\boldsymbol{U}}_{\text{bc}}$, i.e., $\boldsymbol{U}_{\text{sq}}=q\{\boldsymbol{U}_{\text{bc}}\}$. This results in a new initial sphere with radius $\rho_{\text{sq}}^2=\|\boldsymbol{H}\boldsymbol{U}_{\text{sq}}-\bar{\boldsymbol{U}}_{\text{bc}}\|_2^2$. Clearly, during transients $\rho_{\text{sq}}^2\ll\rho_{\text{ini}}^2$, which allows the SDA to quickly discard vectors that are outside this sphere, and thus, achieving a real-time implementation of MS-MPC throughout the whole converter operation. This box-constrained preconditioning approach has been successfully implemented in electrical drives [70] and grid-connected applications [79].

For instance, results for a grid-connected three-level MLI tested under a step change in the current are shown in Fig. 13. For comparison purposes, these results are taken using Processor-in-the-Loop (PiL) simulation with and without a suitable SDA initialization for transients.

Considering a real scenario, i.e., with limited control hardware capabilities, if no action is taken over the exponential

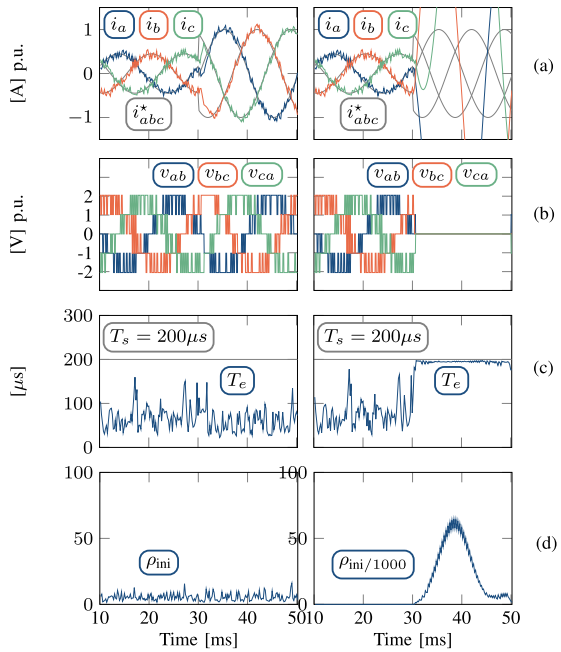

FIGURE 13. PiL-simulation results for $N = 6$ in a 3L grid-connected MLI using a suitable box-constrained based preconditioning approach as in [79] (left) and a standard SDA initialization (right). a) phase currents; b) line-to-line voltages; c) Execution time; d) initial sphere radius.

increment in ρ_{ini}, then the SDA stops and gives a nondeterministic result. This result can be any solution that is on the execution path just before falling into task overrun ($T_e > T_s$). Thus, any output voltage may be applied by the inverter. This leads to grid current instabilities after the step change, demonstrating the importance of resolving challenges associated with transients in MS-MPC; see [79] for further details.

IV. OPERATION WITH FIXED SWITCHING FREQUENCY

From a control perspective, when active control of the capacitor voltage balance is required, the converter model results in a nonlinear system due to the interaction of the states (capacitor voltages) and inputs (semiconductor gate signals), as shown in (1). In general, a standard approach in power electronics to address this issue is to decouple this problem by means of a PWM technique [81]. For example, in [82], [83], and [84], it has been shown that using PS-PWM during steady state the floating capacitors tend to stabilize their voltages without requiring an active control. However, this natural balance mechanism presents a poor capacitor voltage dynamic and large oscillations, which only depends on the system parameters. In MPC algorithms (see, e.g., [36], [85]), the control input is chosen to minimize a cost function, which quantifies a tracking error. An advantage of FCS-MPC methods is that the cost function can merge in a single-expression electrical and nonelectrical variables, e.g., tracking of currents; the balancing of capacitor voltages and the total number of commutation events [86], [87]. However, a clear disadvantage when compared to PWM-based control strategies is that it

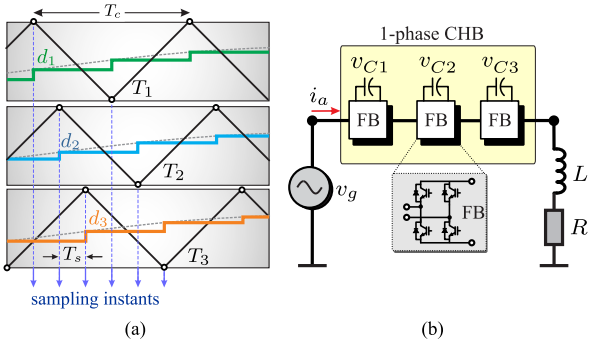

FIGURE 14. (a) Standard PS-PWM working in a double update mode. (b) Single-phase seven-level CHB converter.

produces a variable switching frequency, an uneven distribution of semiconductor losses, and a spread spectrum in the electrical variables.

To address the above issues, a sequential PS MPC (PS-MPC) was proposed in [88] for multicell power converters. This emergent control strategy has been extended for active NPC converter [89], CHB converters [90], [91], and modular multilevel converters [92], [93]. The concepts of the control strategy will be explained by utilizing a single-phase seven-level CHB with floating capacitors, which is illustrated in Fig. 14(b).

In this context, to formulate the sequential PS-MPC strategy, we take advantage of the PS-PWM operating principle [94]. In Fig. 14(a), a three-carrier PS-PWM working in a double update mode is depicted. Here, one can see that each duty cycle d_j is only updated whenever the value of its associated carrier T_j is at one of its edges. After that, d_j remains constant until the next update (i.e., during half of the carrier period $T_c/2$). As shown in Fig. 14(a), this results in a sequential duty cycle update process, with the advantage that only one of them needs to be obtained at each sampling instant. Based on the above analysis, a sequential average model of the converter can be derived.

To this end, the model of the single-phase system depicted in Fig. 14(b) is described by the state and input vectors, which are, respectively, defined as

$$\boldsymbol{x} = \begin{bmatrix} i_a & v_{C1} & v_{C2} & v_{C3} \end{bmatrix}^{\mathrm{T}} \tag{30}$$

$$\boldsymbol{u} = \begin{bmatrix} d_1 & d_2 & d_3 \end{bmatrix}^{\mathrm{T}}. \tag{31}$$

Consequently, the discrete-time model is given by

$$\boldsymbol{x}(k+1) = \mathbf{A}\boldsymbol{x}(k) + \mathbf{B}(\boldsymbol{x}(k))\boldsymbol{u}(k) + \boldsymbol{g}(k) \tag{32}$$

where $\mathbf{A}$ is the state matrix and $\boldsymbol{g}(k) = T_s\begin{bmatrix} v_g/L & 0 \end{bmatrix}^{\mathrm{T}}$. Moreover, the input matrix is given by

$$\mathbf{B}(\boldsymbol{x}(k)) = \begin{bmatrix} -\frac{1}{L}v_{C1}(k) & -\frac{1}{L}v_{C2}(k) & -\frac{1}{L}v_{C3}(k) \\ \frac{1}{C}i_a(k) & 0 & 0 \\ 0 & \frac{1}{C}i_a(k) & 0 \\ 0 & 0 & \frac{1}{C}i_a(k) \end{bmatrix}. \tag{33}$$

Thus, by taking into account that only the ℓth duty cycle is updated at the kth sampling instant, namely, $d_\ell(k)$, the resulting sequential average model of a single-phase seven-level CHB converter is represented via

$$\boldsymbol{x}(k+1) = \mathbf{A}\boldsymbol{x}(k) + \mathbf{b}_\ell(\boldsymbol{x}(k))d_\ell(k) + \boldsymbol{h}_\ell(\boldsymbol{x}(k)) \tag{34}$$

where $\mathbf{b}_j(k)$ is the jth column vector of the input matrix given in (33), and $\boldsymbol{h}_\ell(\boldsymbol{x}(k))$ is a known disturbance given by

$$\boldsymbol{h}_\ell(\boldsymbol{x}(k)) = \boldsymbol{g}(k) + \sum_{\forall j \neq \ell} \mathbf{b}_j(\boldsymbol{x}(k))d_j(k-1). \tag{35}$$

Therefore, according to (34), the future behavior of $\boldsymbol{x}(k+1)$ only depends on the scalar variable $d_\ell(k)$.

To sequentially obtain the optimal duty cycle, the following cost function is introduced:

$$J_\ell(k) = \boldsymbol{e}(k+1)^{\mathrm{T}}\mathbf{Q}\,\boldsymbol{e}(k+1) + \lambda_u\left(d_\ell(k) - d^\star(k)\right)^2 \tag{36}$$

where $\boldsymbol{e}(k+1) = \boldsymbol{x}(k+1) - \boldsymbol{x}^\star(k+1)$ is the next step tracking error and $d^\star(k)$ is the control input allowing to obtain the steady-state equilibrium point [95]. Thus, the optimal duty cycle $d_\ell^{\mathrm{opt}}(k)$ can be directly obtained by using the following explicit optimal solution:

$$d_\ell^{\mathrm{opt}}(k) = -(W_\ell(k))^{-1}F_\ell(k) \tag{37}$$

where

$$\begin{aligned} W_\ell(k) &= \mathbf{b}_\ell(\boldsymbol{x})^{\mathrm{T}}\mathbf{Q}\mathbf{b}_\ell(\boldsymbol{x}) + \lambda_u \\ F_\ell(k) &= \mathbf{b}_\ell(\boldsymbol{x})^{\mathrm{T}}\mathbf{Q}(\mathbf{A}\boldsymbol{x} + \boldsymbol{h}_\ell(\boldsymbol{x}) - \boldsymbol{x}^\star(k+1)) - \lambda_u d^\star \end{aligned} \tag{38}$$

with $\boldsymbol{x} = \boldsymbol{x}(k)$ and $d^\star = d^\star(k)$. Notice that if λ_u is too large, then the second term in (36) becomes predominant. Thus, the optimal solution becomes $d^{\mathrm{opt}}(k) = d^\star(k)$, resulting in an open-loop slow dynamic given by the natural dynamic of the system. On the other hand, if λ_u is too small, then the controller will become in a multivariable deadbeat controller [96], which can be too aggressive. Therefore, λ_u can be used to regulate the closed-loop dynamic.

It is important to emphasize that the introduced sequential PS-MPC strategy can be easily extended to govern three-phase multicell converters with many cells, such as CHBs. In that case, the optimal control problem underlying the sequential PS-MPC controller can be formulated to determine one duty cycle per phase. Thus, for the three-phase CHB converter, the variable to be optimized is given by

$$\boldsymbol{d}_\ell(k) = \left[d_{a\ell}(k)\; d_{b\ell}(k)\; d_{c\ell}(k)\right]^{\mathrm{T}} \in \mathbb{D}^3 \triangleq [-1, 1]^3 \subset \mathbb{R}^3. \tag{39}$$

Therefore, to find the optimal solution, a box-constrained optimization algorithm should be implemented to get the solution efficiently. However, the saturated unconstrained solution performs well, as demonstrated in [90]. The experimental results shown in Fig. 15 validate the high-quality performance of the PS-MPC applied to grid-connected CHB converters.

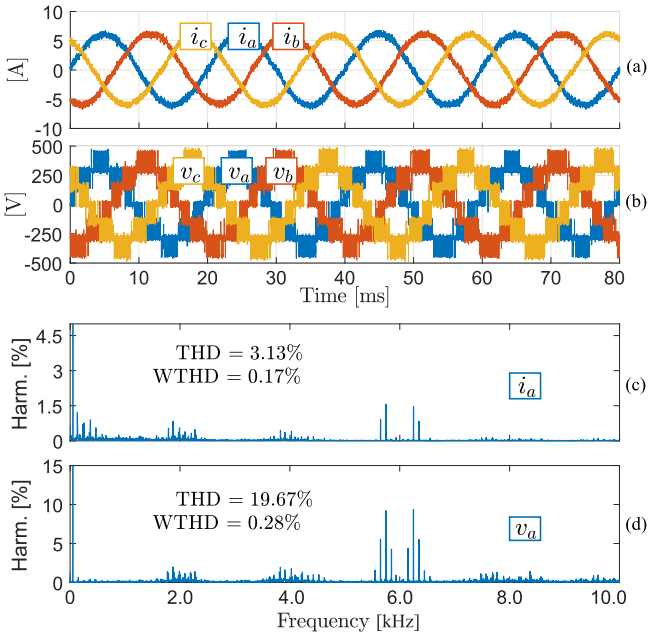

FIGURE 15. Experimental results of PS-MPC applied to CHB. (a) Phase currents. (b) Converter voltages. (c) Current spectra. (d) Converter voltage spectra [90].

V. CONCLUSION

MLIs is a field of increasing importance in power electronics, due to the expanding areas of application that cover from very high power to low power. This is related to the simple implementation of MPC even in complex systems, such as MLIs, linking directly the basic equations of the inverter topology with the control strategy. However, the interest of using MPC in MLIs faced the problem of the very high number of calculations that turned this control strategy not feasible for high number of levels. This article show advances in literature in mitigating this problem by reducing the number of calculations, without deteriorating the performance and the quality of the load voltage. The example of an FC converter has been taken as a study case. From the basic strategy description as well as from the reviewed advanced techniques it can be concluded that the topology complexity is not anymore a limitation to apply MPC. This also applies to other common issues with MPC, as the calculation of the weighting factors. As an example, a strategy has been presented to control the load currents, keeping the capacitor voltages balanced, without using weighting factors. Similar conclusion are obtained when MPC is implemented for CHB converters and advanced technique to reduce the number of switch commutations are presented. Also, a recently proposed technique, named MS-MPC has been reviewed as promising future advance in MPC application to power electronics. Finally, it can be concluded that, while the original problems for using MPC in MLIs can be considered solved, MPC implementation still depends on the quality of the model to perform well. In fact, errors in the parameters and in the models, deteriorate the performance of the control strategy. For this reason, an important area of

future research is to improve the robustness in response to parameter changes or uncertainties in the models. The use of observers and modern techniques like artificial intelligence can improve performance and will open a completely new research area. Another challenge is reliable operation in front of a very large number of power semiconductors, typical in MLIs. Here, future research work must consider the possibility of failure of some components and use the property of redundancy with intelligent strategies to modify the MPC to maintain the operation of the inverter.

REFERENCES

[1] J. Rodriguez, J.-S. Lai, and F. Z. Peng, "Multilevel inverters: A survey of topologies, controls, and applications," *IEEE Trans. Ind. Electron.*, vol. 49, no. 4, pp. 724–738, Aug. 2002.

[2] H. Akagi, "Classification, terminology, and application of the modular multilevel cascade converter (MMCC)," *IEEE Trans. Power Electron.*, vol. 26, no. 11, pp. 3119–3130, Nov. 2011.

[3] H. Abu-Rub, J. Holtz, J. Rodriguez, and G. Baoming, "Medium-voltage multilevel convertersstate of the art, challenges, and requirements in industrial applications," *IEEE Trans. Ind. Electron.*, vol. 57, no. 8, pp. 2581–2596, Aug. 2010.

[4] J. Rodriguez, S. Bernet, B. Wu, J. O. Pontt, and S. Kouro, "Multilevel voltage-source-converter topologies for industrial medium-voltage drives," *IEEE Trans. Ind. Electron.*, vol. 54, no. 6, pp. 2930–2945, Dec. 2007.

[5] P. Vivek and N. Muthuselvan, "Investigation on photovoltaic system based asymmetrical multilevel inverter for harmonic mitigation," in *Proc. 7th Int. Conf. Elect. Energy Syst.*, Feb. 2021, pp. 334–339.

[6] D. K. Singh, S. Manna, and A. Akella, "Grid connected PV system using multilevel inverter," in *Proc. 7th Int. Conf. Elect. Energy Syst.*, Feb. 2021, pp. 346–351.

[7] P. Chamarthi, A. Al-Durra, T. H. El-Fouly, and K. A. A. Jaafari, "A novel three-phase transformerless cascaded multilevel inverter topology for grid-connected solar PV applications," *IEEE Trans. Ind. Appl.*, vol. 57, no. 3, pp. 2285–2297, May/Jun. 2021.

[8] S. R. Khasim, D. C. S. Padmanaban, J. B. Holm-Nielsen, and M. Mitolo, "A novel asymmetrical 21-level inverter for solar PV energy system with reduced switch count," *IEEE Access*, vol. 9, pp. 11761–11775, 2021.

[9] S. Dhara, A. Hota, S. Jain, and V. Agarwal, "A transformerless 1-φ, 5-level half-bridge PV inverter configuration based on switched-capacitor technique," *IEEE Trans. Ind. Appl.*, vol. 57, no. 2, pp. 1619–1628, Mar./Apr. 2021.

[10] K. Ishibashi and H. Yamada, "Modular multilevel converter based single-phase grid-tied wind power generation system with multiple wind power generators under different wind speeds," in *Proc. 23rd Int. Conf. Elect. Machines Syst.*, Nov. 2020, pp. 1017–1021.

[11] E. Oumaymah, O. Abdellah, and E. A. Mustapha, "The injection of wind power into a grid using a multi-level inverter controlled by SVPWM," in *Proc. Int. Conf. Elect. Inf. Technol.*, Mar. 2020, pp. 1–6.

[12] A. Poorfakhraei, M. Narimani, and A. Emadi, "A review of modulation and control techniques for multilevel inverters in traction applications," *IEEE Access*, vol. 9, pp. 24187–24204, 2021.

[13] C. Dhanamjayulu, S. Padmanaban, V. K. Ramachandaramurthy, J. B. Holm-Nielsen, and F. Blaabjerg, "Design and implementation of multilevel inverters for electric vehicles," *IEEE Access*, vol. 9, pp. 317–338, 2021.

[14] B. C. Chakravarthi, P. Naveen, S. Pragaspathy, and V. S. N. N. Raju, "Performance of induction motor with hybrid multi level inverter for electric vehicles," in *Proc. Int. Conf. Artif. Intell. Smart Syst.*, Mar. 2021, pp. 1474–1478.

[15] H. P. Vemuganti, D. Sreenivasarao, S. K. Ganjikunta, H. M. Suryawanshi, and H. Abu-Rub, "A survey on reduced switch count multilevel inverters," *IEEE Open J. Ind. Electron. Soc.*, vol. 2, pp. 80–111, 2021.

[16] A. Iqbal, M. D. Siddique, B. P. Reddy, and P. K. Maroti, "Quadruple boost multilevel inverter (QB-MLI) topology with reduced switch count," *IEEE Trans. Power Electron.*, vol. 36, no. 7, pp. 7372–7377, Jul. 2021.

[17] A. Salem, H. V. Khang, K. G. Robbersmyr, M. Norambuena, and J. Rodriguez, "Voltage source multilevel inverters with reduced device count: Topological review and novel comparative factors," *IEEE Trans. Power Electron.*, vol. 36, no. 3, pp. 2720–2747, Mar. 2021.

[18] B. S. Naik, Y. Suresh, J. Venkataramanaiah, and A. K. Panda, "A hybrid nine-level inverter topology with boosting capability and reduced component count," *IEEE Trans. Circuits Syst. II, Exp. Briefs*, vol. 68, no. 1, pp. 316–320, Jan. 2021.

[19] W. Lin, J. Zeng, J. Hu, and J. Liu, "Hybrid nine-level boost inverter with simplified control and reduced active devices," *IEEE Trans. Emerg. Sel. Topics Power Electron.*, vol. 9, no. 2, pp. 2038–2050, Apr. 2021.

[20] B. McGrath and D. Holmes, "Multicarrier PWM strategies for multilevel inverters," *IEEE Trans. Ind. Electron.*, vol. 49, no. 4, pp. 858–867, Aug. 2002.

[21] P. Lingom, J. Song-Manguelle, R. C. Flesch, and T. Jin, "A generalized single-carrier PWM scheme for multilevel converters," *IEEE Trans. Power Electron.*, vol. 36, no. 10, pp. 12112–12126, 2021.

[22] Y. Kumar, A. Saxena, and M. Goyal, "Integration of hybrid cascaded multilevel inverter configuration in a PV based applications with multicarrier PWM technology," in *Proc. Int. Conf. Adv. Electrical, Comput., Commun. Sustain. Technol.*, 2021, pp. 1–5.

[23] S. K. Annam, R. K. Pongiannan, and N. Yadaiah, "A hysteresis space vector PWM for PV tied z-source NPC-MLI with DC-link neutral point balancing," *IEEE Access*, vol. 9, pp. 54420–54434, 2021.

[24] P. Kant and B. Singh, "A sensorless DTC scheme for 60-pulse AC-DC converter fed 5-level six-leg NPC inverter based medium voltage induction motor drive," *IEEE Trans. Energy Convers.*, vol. 35, no. 4, pp. 1916–1925, Dec. 2020.

[25] M. P. Thakre and P. S. Borse, "Analytical evaluation of FOC and DTC induction motor drives in three levels and five levels diode clamped inverter," in *Proc. Int. Conf. Power, Energy, Control Transmiss. Syst.*, 2020, pp. 1–6.

[26] J. E. Huber and A. J. Korn, "Optimized pulse pattern modulation for modular multilevel converter high-speed drive," in *Proc. 15th Int. Power Electron. Motion Control Conf.*, Sep. 2012, pp. LS1a-1.4-1–LS1a-1.4-7.

[27] M. Mehrasa, M. Babaie, A. Zafari, and K. Al-Haddad, "Passivity ANFIS-based control for an intelligent compact multilevel converter," *IEEE Trans. Ind. Inform.*, vol. 17, no. 8, pp. 5141–5151, Aug. 2021.

[28] M. Babaie, M. Sharifzadeh, H. Y. Kanaan, and K. Al-Haddad, "Switching-based optimized sliding-mode control for capacitor self-voltage balancing operation of seven-level PUC inverter," *IEEE Trans. Ind. Electron.*, vol. 68, no. 4, pp. 3044–3057, Apr. 2021.

[29] A. Krama, S. S. Refaat, and H. Abu-Rub, "A robust second-order sliding mode control of sensorless five level packed U cell inverter," in *Proc. 46th Annu. Conf. IEEE Ind. Electron. Soc.*, Oct. 2020, pp. 2412–2417.

[30] V. Patel, S. D. Gennaro, C. Buccella, and C. Cecati, "Super twisting sliding mode controller for PMSM fed with multilevel inverter for e-transportation," in *Proc. IEEE 9th Int. Power Electron. Motion Control Conf.*, 2020, pp. 238–244.

[31] M. Babaie, M. Sharifzadeh, M. Mehrasa, and K. Al-Haddad, "Lyapunov based neural network estimator designed for grid-tied nine-level packed e-cell inverter," in *Proc. IEEE Appl. Power Electron. Conf. Expo.*, 2020, pp. 3311–3315.

[32] M. Manoharsha, B. Babu, K. Veeresham, and R. Kapoor, "ANN based selective harmonic elimination for cascaded H-bridge multilevel inverter," in *Proc. 7th Int. Conf. Elect. Energy Syst.*, 2021, pp. 183–188.

[33] V. Eslampanah, R. Ebrahimi, M. Azizian, and H. M. Kojabadi, "Artificial neural networks for control of three phase grid connected t-type inverter," in *Proc. 28th Iranian Conf. Elect. Eng.*, Aug. 2020, pp. 1–6.

[34] S. Kouro, P. Cortes, R. Vargas, U. Ammann, and J. Rodriguez, "Model predictive control—A simple and powerful method to control power converters," *IEEE Trans. Ind. Electron.*, vol. 56, no. 6, pp. 1826–1838, Jun. 2009.

[35] J. Rodriguez et al., "State of the art of finite control set model predictive control in power electronics," *IEEE Trans. Ind. Inform.*, vol. 9, no. 2, pp. 1003–1016, May 2013.

[36] S. Vazquez, J. Rodriguez, M. Rivera, L. G. Franquelo, and M. Norambuena, "Model predictive control for power converters and drives: Advances and trends," *IEEE Trans. Ind. Electron.*, vol. 64, no. 2, pp. 935–947, Feb. 2017.

[37] P. Karamanakos, E. Liegmann, T. Geyer, and R. Kennel, "Model predictive control of power electronic systems: Methods, results, and challenges," *IEEE Open J. Ind. Appl.*, vol. 1, pp. 95–114, 2020.

[38] J. O. Krah, T. Schmidt, and J. Holtz, "Predictive current control with synchronous optimal pulse patterns," in *Proc. 2nd Int. Conf. Smart Grid Renewable Energy*, Nov. 2019, pp. 1–6.

[39] T. Geyer, G. Papafotiou, and M. Morari, "Model predictive direct torque control Part I: Concept, algorithm, and analysis," *IEEE Trans. Ind. Electron.*, vol. 56, no. 6, pp. 1894–1905, Jun. 2009.

[40] M. F. Elmorshedy, W. Xu, F. F. M. El-Sousy, M. R. Islam, and A. A. Ahmed, "Recent achievements in model predictive control techniques for industrial motor: A comprehensive state of the art," *IEEE Access*, vol. 9, pp. 58170–58191, 2021.

[41] G. Darivianakis, T. Geyer, and W. van der Merwe, "Model predictive current control of modular multilevel converters," in *Proc. IEEE Energy Convers. Congr. Expo.*, 2014, pp. 5016–5023. [Online]. Available: https://doi.org/10.1109/ecce.2014.6954089

[42] M. Najjar, M. Shahparasti, R. Heydari, and M. Nymand, "Model predictive controllers with capacitor voltage balancing for a single-phase five-level SiC/si based ANPC inverter," *IEEE Open J. Power Electron.*, vol. 2, pp. 202–211, 2021.

[43] J. Raath, T. Mouton, and T. Geyer, "Alternative sphere decoding algorithm for long-horizon model predictive control of multi-level inverters," in *Proc. IEEE 21st Workshop Control Model. Power Electron.*, 2020, pp. 1–8.

[44] K. Bandy and P. Stumpf, "Model predictive torque control for multilevel inverter fed induction machines using sorting networks," *IEEE Access*, vol. 9, pp. 13800–13813, 2021.

[45] M. Wu, H. Tian, Y. W. Li, G. Konstantinou, and K. Yang, "A composite selective harmonic elimination model predictive control for seven-level hybrid-clamped inverters with optimal switching patterns," *IEEE Trans. Power Electron.*, vol. 36, no. 1, pp. 274–284, Jan. 2021.

[46] M. Aly, F. Carnielutti, M. Norambuena, S. Kouro, and J. Rodriguez, "A model predictive control method for common grounded photovoltaic multilevel inverter," in *Proc. 46th Annu. Conf. IEEE Ind. Electron. Soc.*, 2020, pp. 2401–2406.

[47] R. O. Ramirez, C. R. Baier, F. Villarroel, J. R. Espinoza, J. Pou, and J. Rodriguez, "A hybrid FCS-MPC with low and fixed switching frequency without steady-state error applied to a grid-connected CHB inverter," *IEEE Access*, vol. 8, pp. 223637–223651, 2020.

[48] S. R. Mohapatra and V. Agarwal, "A low computational cost model predictive controller for grid connected three phase four wire multilevel inverter," in *Proc. IEEE 27th Int. Symp. Ind. Electron.*, IEEE, Jun. 2018, pp. 305–310.

[49] B. Gutierrez and S.-S. Kwak, "Model predictive control method with preselected control options for reduced computational complexity in modular multilevel converters (MMCS)," in *Proc. 20th Eur. Conf. Power Electron. Appl.*, 2018, pp. P.1–P.8.

[50] I. Harbi et al., "Model predictive control of multilevel inverters: Challenges, recent advances, and trends," *IEEE Trans. Power Electron.*, vol. 38, no. 9, pp. 10845–10868, Sep. 2023.

[51] A. Ortiz, P. Lezana, and M. Norambuena, "Two stages FCS-MPC for a flying capacitor converter with improved switching performance," *IEEE Trans. Ind. Inform.*, vol. 20, no. 6, pp. 8358–8367, Jun. 2024.

[52] Y. Yang et al., "Multiple-voltage-vector model predictive control with reduced complexity for multilevel inverters," *IEEE Trans. Transport. Electrific.*, vol. 6, no. 1, pp. 105–117, Mar. 2020.

[53] R. Amir, A. Hasan, and O. Hasan, "Approximate sphere decoding based model predictive control of cascaded H-bridge inverters," in *Proc. IEEE 13th Int. Conf. Compat., Power Electron. Power Eng.*, 2019, pp. 1–6.

[54] Y. Zhang, X. Wu, X. Yuan, Y. Wang, and P. Dai, "Fast model predictive control for multilevel cascaded H-bridge STATCOM with polynomial computation time," *IEEE Trans. Ind. Electron.*, vol. 63, no. 8, pp. 5231–5243, Aug. 2016.

[55] Y. Zhang, X. Wu, and X. Yuan, "A simplified branch and bound approach for model predictive control of multilevel cascaded H-bridge STATCOM," *IEEE Trans. Ind. Electron.*, vol. 64, no. 10, pp. 7634–7644, Oct. 2017.

[56] Z. Ni and M. Narimani, "A new fast formulation of model predictive control for CHB STATCOM," in *Proc. 45th Annu. Conf. IEEE Ind. Electron. Soc.*, vol. 1, 2019, pp. 3493–3498.

[57] Z. Ni and M. Narimani, "A new model predictive control formulation for CHB inverters," in *Proc. IEEE Appl. Power Electron. Conf. Expo.*, 2020, pp. 2462–2466.

[58] Z. Ni, A. Abuelnaga, and M. Narimani, "A novel high-performance predictive control formulation for multilevel inverters," *IEEE Trans. Power Electron.*, vol. 35, no. 11, pp. 11533–11543, Nov. 2020.

[59] I. Kim, R. Chan, and S. Kwak, "Model predictive control method for CHB multi-level inverter with reduced calculation complexity and fast dynamics," *IET Electric Power Appl.*, vol. 11, no. 5, pp. 784–792, 2017.

[60] A. Mora, R. Cárdenas-Dobson, R. P. Aguilera, A. Angulo, F. Donoso, and J. Rodriguez, "Computationally efficient cascaded optimal switching sequence MPC for grid-connected three-level NPC converters," *IEEE Trans. Power Electron.*, vol. 34, no. 12, pp. 12464–12475, Dec. 2019.

[61] A. Mora, R. Cardenas, R. P. Aguilera, A. Angulo, P. Lezana, and D. D.-C. Lu, "Predictive optimal switching sequence direct power control for grid-tied 3L-NPC converters," *IEEE Trans. Ind. Electron.*, vol. 68, no. 9, pp. 8561–8571, Sep. 2021.

[62] S. Vazquez et al., "Model predictive control for single-phase NPC converters based on optimal switching sequences," *IEEE Trans. Ind. Electron.*, vol. 63, no. 12, pp. 7533–7541, Dec. 2016.

[63] S. Vazquez, P. Acuna, R. P. Aguilera, J. Pou, J. I. Leon, and L. G. Franquelo, "Dc-link voltage-balancing strategy based on optimal switching sequence model predictive control for single-phase H-NPC converters," *IEEE Trans. Ind. Electron.*, vol. 67, no. 9, pp. 7410–7420, Sep. 2020.

[64] D. Schuetz, F. Carnielutti, M. Aly, M. Norambuena, J. Rodriguez, and H. Pinheiro, "Fast finite control set model predictive control for multilevel inverters," in *Proc. IEEE Int. Conf. Predictive Control Elect. Drives Power Electron.*, 2021, pp. 29–34.

[65] D. Schuetz et al., "Space vector modulated model predictive control for grid-tied converters," *IEEE Trans. Ind. Inform.*, vol. 19, no. 1, pp. 414–425, Jan. 2023.

[66] J. D. Barros, J. F. A. Silva, and G. A. Jesus, "Fast-predictive optimal control of NPC multilevel converters," *IEEE Trans. Ind. Electron.*, vol. 60, no. 2, pp. 619–627, Feb. 2013.

[67] S. R. Mohapatra and V. Agarwal, "Model predictive controller with reduced complexity for grid-tied multilevel inverters," *IEEE Trans. Ind. Electron.*, vol. 66, no. 11, pp. 8851–8855, Nov. 2019.

[68] P. Karamanakos and T. Geyer, "Guidelines for the design of finite control set model predictive controllers," *IEEE Trans. Power Electron.*, vol. 35, no. 7, pp. 7434–7450, Jul. 2020.

[69] T. Geyer, *Model Predictive Control of High Power Converters and Industrial Drives*. Chichester, U.K.: Wiley, 2016.

[70] P. Acuna, C. A. Rojas, R. Baidya, R. P. Aguilera, and J. E. Fletcher, "On the impact of transients on multistep model predictive control for medium-voltage drives," *IEEE Trans. Power Electron.*, vol. 34, no. 9, pp. 8342–8355, Sep. 2019.

[71] R. H. Cuzmar, A. Mora, J. Pereda, P. Poblete, and R. P. Aguilera, "Long-horizon sequential FCS-MPC approaches for modular multilevel matrix converters," *IEEE Trans. Ind. Electron.*, vol. 71, no. 5, pp. 5137–5147, May 2024.

[72] R. Baidya, R. P. Aguilera, P. Acuña, S. Vazquez, and H. d. T. Mouton, "Multistep model predictive control for cascaded H-bridge inverters: Formulation and analysis," *IEEE Trans. Power Electron.*, vol. 33, no. 1, pp. 876–886, Jan. 2018.

[73] T. Geyer, P. Karamanakos, and R. Kennel, "On the benefit of long-horizon direct model predictive control for drives with LC filters," in *Proc. IEEE Energy Convers. Congr. Expo.*, 2014, pp. 3520–3527.

[74] M. Rossi, P. Karamanakos, and F. Castelli-Dezza, "An indirect model predictive control method for grid-connected three-level neutral point clamped converters with *LCL* filters," *IEEE Trans. Ind. Appl.*, vol. 58, no. 3, pp. 3750–3768, May/Jun. 2022.

[75] E. Liegmann, P. Karamanakos, and R. Kennel, "Real-time implementation of long-horizon direct model predictive control on an embedded system," *IEEE Open J. Ind. Appl.*, vol. 3, pp. 1–12, 2022.

[76] E. Zafra et al., "Parallel sphere decoding algorithm for long-prediction-horizon FCS-MPC," *IEEE Trans. Power Electron.*, vol. 37, no. 7, pp. 7896–7906, Jul. 2022.

[77] E. Zafra, S. Vazquez, A. M. Alcaide, L. G. Franquelo, J. I. Leon, and E. P. Martin, "K-best sphere decoding algorithm for long prediction horizon FCS-MPC," *IEEE Trans. Ind. Electron.*, vol. 69, no. 8, pp. 7571–7581, Aug. 2022.

[78] T. Dorfling, H. du Toit Mouton, T. Geyer, and P. Karamanakos, "Long-horizon finite-control-set model predictive control with nonrecursive sphere decoding on an FPGA," *IEEE Trans. Power Electron.*, vol. 35, no. 7, pp. 7520–7531, Jul. 2020.

[79] R. Baidya et al., "Enabling multistep model predictive control for transient operation of power converters," *IEEE Open J. Ind. Electron. Soc.*, vol. 1, pp. 284–297, 2020.

[80] R. Baidya et al., "Dealing with suboptimality in multistep model predictive control for transient operations," in *Proc. IEEE Energy Convers. Congr. Expo.*, 2019, pp. 3780–3785.
[81] J. I. Leon, S. Kouro, L. G. Franquelo, J. Rodríguez, and B. Wu, "The essential role and the continuous evolution of modulation techniques for voltage-source inverters in the past, present, and future power electronics," *IEEE Trans. Ind. Electron.*, vol. 63, no. 5, pp. 2688–2701, May 2016.
[82] R. H. Wilkinson, T. A. Meynard, and H. du Toit Mouton, "Natural balance of multicell converters: The general case," *IEEE Trans. Power Electron.*, vol. 21, no. 6, pp. 1658–1666, Nov. 2006.
[83] B. McGrath and D. Holmes, "Analytical modelling of voltage balance dynamics for a flying capacitor multilevel converter," *IEEE Trans. Power Electron.*, vol. 23, no. 2, pp. 543–550, Mar. 2008.
[84] B. McGrath and D. Holmes, "Natural capacitor voltage balancing for a flying capacitor converter induction motor drive," *IEEE Trans. Power Electron.*, vol. 24, no. 6, pp. 1554–1561, Jun. 2009.
[85] A. Mora et al., "Model-predictive-control-based capacitor voltage balancing strategies for modular multilevel converters," *IEEE Trans. Ind. Electron.*, vol. 66, no. 3, pp. 2432–2443, Mar. 2019.
[86] R. Vargas, U. Ammann, and J. Rodríguez, "Predictive approach to increase efficiency and reduce switching losses on matrix converters," *IEEE Trans. Power Electron.*, vol. 24, no. 4, pp. 894–902, Apr. 2009.
[87] V. Yaramasu, M. Rivera, M. Narimani, B. Wu, and J. Rodríguez, "Model predictive approach for a simple and effective load voltage control of four-leg inverter with an output *LC* filter," *IEEE Trans. Ind. Electron.*, vol. 61, no. 10, pp. 5259–5270, Oct. 2014.
[88] R. P. Aguilera, P. Acuna, X. Su, P. Lezana, and B. McGrath, "Sequential phase-shifted model predictive control for multicell power converters," in *Proc. IEEE Southern Power Electron. Conf.*, 2017, pp. 1–6.
[89] A. Mora, R. P. Aguilera, R. Cárdenas, P. Lezana, and D. D. C. Lu, "Phase-shifted model predictive control of a three-level active-NPC converter," in *Proc. IEEE 27th Int. Symp. Ind. Electron.*, 2018, pp. 270–276.
[90] R. Cuzmar, J. Pereda, and R. P. Aguilera, "Phase-shifted model predictive control to achieve power balance of CHB converters for large-scale photovoltaic integration," *IEEE Trans. Ind. Electron.*, vol. 68, no. 10, pp. 9619–9629, Oct. 2021.
[91] S. Neira, P. Poblete, R. Cuzmar, J. Pereda, and R. P. Aguilera, "Sequential phase-shifted model predictive control for a multilevel converter with integrated battery energy storage," in *Proc. IEEE 11th Int. Symp. Power Electron. Distrib. Gener. Syst.*, 2020, pp. 29–34.
[92] P. Poblete, S. Neira, R. P. Aguilera, J. Pereda, and J. Pou, "Sequential phase-shifted model predictive control for modular multilevel converters," *IEEE Trans. Energy Convers.*, vol. 36, no. 4, pp. 2691–2702, Dec. 2021.
[93] R. H. Cuzmar, A. Mora, J. Pereda, R. P. Aguilera, P. Poblete, and S. Neira, "Computationally efficient MPC for modular multilevel matrix converters operating with fixed switching frequency," *IEEE Open J. Ind. Electron. Soc.*, vol. 4, pp. 748–761, 2023.
[94] R. P. Aguilera et al., "Selective harmonic elimination model predictive control for multilevel power converters," *IEEE Trans. Power Electron.*, vol. 32, no. 3, pp. 2416–2426, Mar. 2017.
[95] R. P. Aguilera, P. Lezana, and D. E. Quevedo, "Finite-control-set model predictive control with improved steady-state performance," *IEEE Trans. Ind. Inform.*, vol. 9, no. 2, pp. 658–667, May 2013.
[96] D. E. Quevedo, R. P. Aguilera, and T. Geyer, "Predictive control in power electronics and drives: Basic concepts, theory, and methods," in *Advanced and Intelligent Control in Power Electronics and Drives*. New York, NY, USA: Springer, 2014, pp. 181–226.